International Journal For Recent Developments in Science & Technology
2581-4575
Crossref
A Peer Reviewed Research Journal

EXTREMELY HIGH RESOLUTION OF SAR IMAGE USING STRIP LAYERING DIAGRAM

Mr. Gude Ramarao[1], Vanam Vyshnavi[2], Vutukuru Supriya[3], Mula Sonali[4], RaaviSonu Sreeya[5],
Associate Professor, [2,3,4,5] UG Scholar,
[1,2,3,4,5]Department of Electronics and Communication Engineering,
[1,2,3,4,5]G. Pullaiah College of Engineering and Technology, Kurnool, India.

Abstract:

For comprehensive data collecting, an extremely high resolution (EHR) spaceborne sliding spotlight synthetic aperture radar (SAR) must use a continuous variable pulse interval (CVPI) sequence. In a pulse train, the best CVPI sequence is the one that results in the least amount of movement of the echoes of interest. However, using the usual timing diagram, such an optimization is difficult to achieve. In order to address this issue, this paper provides a new graphic tool known as the strip layering diagram, which can be used to achieve the best CVPI sequence for an EHR spaceborne sliding spotlight SAR. The main idea is to use a new parameter to control the movement of the echoes of interest in a pulse train explicitly. The new strip layering diagram has two layered sub diagrams: one is the candidate sub diagram, which is made up of candidate strips that show all the CVPI sequence candidates that are restricted by the data acquisition geometry; the other is the feasibility sub diagram, which is made up of feasibility strips that show all the feasible regions where the echoes of interest are not submerged by transmitted pulses or contaminated by nadir echoes. By sketching a line segment that meets four characteristics inside the strip layering diagram, an optimal CVPI sequence can be achieved correctly and effectively. The comparisons between the new diagram and the classic timing diagram are very comprehensive.

I. Introduction

One of the most crucial performance metrics for spaceborne synthetic aperture radar is RESOLUTION (SAR). In general, the greater the resolution, the more detailed the image. A spaceborne SAR can detect the presence of a target, resulting in improved target identification for applications such as catastrophemonitoring,traffic monitoring, and tomographic mapping. The Capella mission, for example, has a resolution of up to 0.018 m. The synthetic aperture generated by the relative movement of a radar antenna to a target determines the azimuth resolution of a spaceborne SAR. In practice, the sliding spotlight mode, which is characterized by a good tradeoff between azimuth resolution and azimuth scene extension by having a footprint speed slower than the speed of satellite, is typically used to achieve a large synthetic aperture.

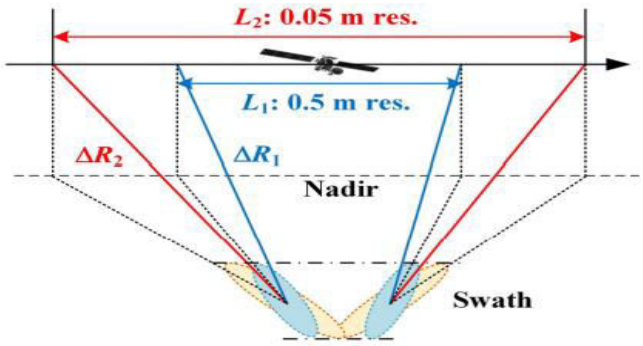

Fig 1: SAR geometries with high azimuth resolution (0.5 m in blue) and extremely high azimuth resolution (0.05 m in red) from spaceborne sliding spotlights.

The better the azimuth resolution, the slower the footprint speed is. When the azimuth resolution is increased to an exceptionally high level, such as from 0.5 to 0.05 m, as shown in Fig. 1, a new issue of developing a good pulse interval (PI) sequence to fully receive the echoes of interest arises. Assume

International Journal For Recent Developments in Science & Technology
2581-4575
Crossref
A Peer Reviewed Research Journal

that the extremely high-resolution (EHR) spaceborne sliding spotlight SAR proposed here uses the decamping on receive technique described. The primary goal of creating a PI sequence is to avoid signal gaps caused by the inability to receive throughout the recording process. High-power nadir echoes can cause jamming or transmit events. A PI sequence, such as the one shown in Fig. 2, has constant intervals and is represented by a vertical line segment in the timing diagram. Only if a uniform PI sequence is fully contained within a diamond-like interval bounded by the blue and red strips is it legitimate.

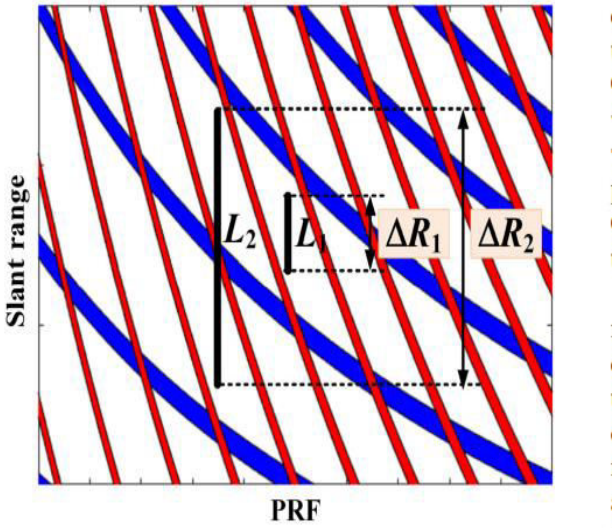

Fig 2: shows a timing diagram with homogeneous PI sequences. R1 and R2 signify the overall slant range difference of the target and the two-way slant range corresponding to pulse duration, respectively.

In the 0.5- and 0.05-m cases in Fig. 1, define R1 and R2 as the total slant range variations of the echoes of interest (the sum of the total slant range difference of target and the two-way slant range corresponding to pulse duration) in the vertical line segments of L1 and L2 in the timing diagram in Fig. 2. R2 is much larger than R1, as L2 is much longer than L1 in Fig. 2, due to the much increased synthetic aperture width. While everything is OK for L1 in Fig. 2, we have the problem that the considerably longer L2 cannot be contained by any diamond-like period, resulting in the loss of portions of the echoes of interest. A nonuniform continuously variable pulse interval might theoretically be used to overcome this problem.(CVPI) is a sequence of letters. It's worth noting that we use the term "PI" here. "Pulse repetition interval (PRI)" instead of "pulse repetition interval (PRI)" to underline that the CVPI sequence of pulses is the collection of all pulses that occur during the CVPI procedure. It is optimized for the sliding spotlight acquisition. The azimuth sampling sequence is not repeated, and no particular structure or regularity is anticipated. The reason behind this is to keep the volatility of the interest echoes within bounds that ensures that the transmission blockage and nadir are not violated situations of ambiguity Assuming we always use a fixed receiving window delay (with relation to the last sent pulse, see g),We want to keep the movement of the object as small as possible (see Fig. 6) interest echoes in a pulse train, in order to finally decrease the entire amount of RAM required for storing As a result, in addition to having a plausible plan, CVPI sequence that satisfies the basic criteria given above. None of them, however, entirely satisfies. The primary criterion for full data collection is that there is none one of them analyses the stifling effect of the strong nadir echoes in the background. PRI strategies that fluctuate cyclically, such as applied for staggered SAR, with the goal of enabling high-resolution wide-swath missions like Tandem-Land NASA-ISRO SAR (NISAR), resolving a problem unrelated to the EHR spaceborne sliding spotlight. Here, SAR is taken into account. A CVPI has yet to be discovered in the literature. To ensure the completeness of data, use a sequence design method. Allow more time for an EHR spaceborne sliding spotlight SAR. Sophisticated optimization for the smallest possible movement. In a pulse train, there are echoes of interest. The purpose of this article is to introduce a new approach for a CVPI sequence that is optimal for an EHR spaceborne sliding SAR should be highlighted in a graphical style. The most important contribution is the development of a new graphical tool known as the correct CVPI sequence can be found on a strip layering diagram Approach beats state-of-the-art methods in a variety of ways. Three points to consider

1) It generates a CVPI sequence that satisfies all of the essential conditions, ensuring that neither the

International Journal For Recent Developments in Science & Technology
2581-4575
Crossref
A Peer Reviewed Research Journal

transmission pulse nor the nadir echo compromise data completeness.

2) The CVPI sequence obtained is the best with the smallest movement of attention echoes in a train of pulses
3) The optimization is carried out in a very efficient and effective manner.

without the need for time-consuming procedures calculations that are repeated.

The strip layering diagram has two levels of sub diagrams for the technical aspect: a candidate sub diagram and a feasibility sub diagram. The former shows all CVPI sequence candidates that are constrained by the data collecting geometry using "candidate strips." The latter denotes CVPI sequences that do not break the "feasibility strips"' basic criteria for complete data capture.The rationale for using a CVPI sequence for an EHR spaceborne sliding spotlight is as follows: Section II delves into SAR. The third section introduces the new detailed schematic of strip layering. The contrast between the two conventional timing diagram and the new strip stacking diagram Section IV is where the action takes place. There are two design examples presented. Section V will be used to validate the approaches that have been provided. VIth Section highlights the findings of this study.

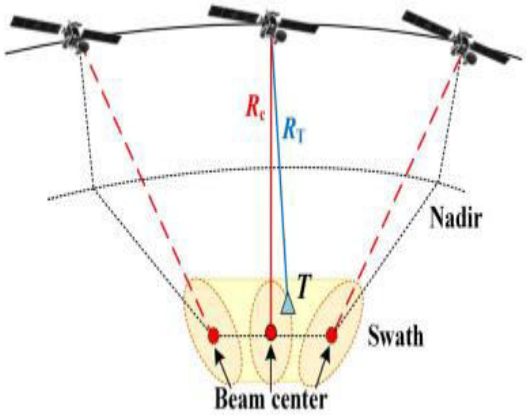

Fig. 3. Geometry of an EHR spaceborne sliding spotlight SAR.

II. Motivation

A. Slant Range History and Geometry

Take, for example, the geometry of an EHR spaceborne sliding spotlight SAR in Fig. 3. The immediate slant range from the antenna phase center to the ground beam center is denoted by Rc. Within the imaging swath, T signifies an arbitrary target. The immediate slant range from the antenna phase center to target T is denoted by RT. The RT of distinct targets fluctuates around Rc at an azimuth time instant due to the elevation footprint, resulting in the total length of the echoes of interest $\tau_w$as

$$\tau_w=T_p+\frac{\Delta R_T}{2} \quad (1)$$

The transmitted pulse width is Tp, and the total variance of RT is RT. Consider a picture in which the azimuth time t is the horizontal axis and the slant range is the vertical axis, as illustrated in Fig. 4, and the elevation beam coverage at a given azimuth time instant is represented by a vertical line segment of length wc/2. We generate a continuous green patch reflecting the complete slant range fluctuation of the echoes of interest by sketching all of these vertical line segments over the entire data acquisition in the diagram. Rc's and an exemplary RT's history are depicted in red and blue, respectively. The total slant range variations of the echoes of interest, R, and the variation of Rc, respectively, are the total slant range variations of the echoes of interest and the variation of Rc.

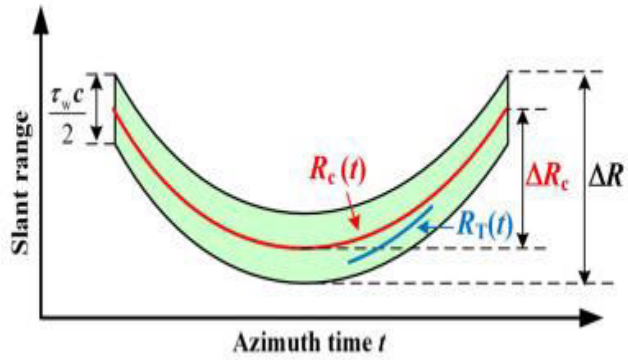

Fig 4: The total slant range variation of the interest echoes.

International Journal For Recent Developments in Science & Technology
2581-4575
Crossref
A Peer Reviewed Research Journal

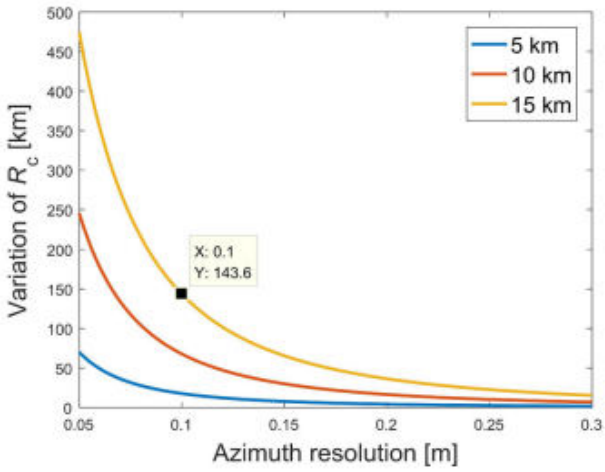

Fig 5: how Rc is affected by azimuth resolution and scene extension.

The vertical span of the green region RT only accounts for a minor portion of the overall slant range change in an EHR case, implying that R is mostly influenced by Rc. This shows that just a narrow echo is received at first (low w), but that as Rc(t) changes over time, the receiving window must have a significant extent (see Fig. 6). The explicit expression of Rc is (A4), which follows the rule that the bigger the azimuth scene extension Wa and the higher the azimuth resolution a, the larger the Rc, as seen in Fig. 5. The length of the path of the beam center on the ground is denoted by Wa. The blue, red, and orange lines represent the 5-, 10-, and 15-kilometer azimuth scene extensions, respectively. Consider a spaceborne sliding spotlight SAR with a wavelength of 0.03 m and a beamwidth of 0.28 azimuth. As seen in the image, imaging a 15-km azimuth scene extension at 0.1-m azimuth resolution results in a Rc of up to 143.6 km.
Assume that in Fig. 6, τc is the period between the centre of an interest echo with the slant range Rc and the centre of the most preceding transmission pulse. A new time-varying parameter can be used to explicitly present the relative position of the echo of interest in a PI, such as

$$\eta(t)=\frac{\tau_c(t)}{PI\,(t)} \quad (2)$$

where P I is the time interval between the previous and subsequent transmitted pulses.

$$\eta=\frac{\tau_c}{PI}$$

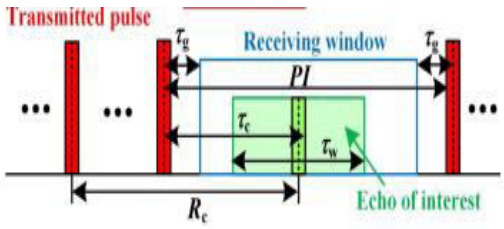

Fig 6: shows the relative position of the echo of interest in a PI, as shown by the parameter of η

The movement of the echoes of interest in a pulse train can be represented by c, as shown in Fig. 6. A large variation of Rc will generate a violent variation of c, resulting in a severe movement of the echoes of interest in a pulse train if a typical PI sequence is used. A valid should satisfy from not being able to be recorded owing to transmission.

$$\frac{\tau_w}{2\,PI}+\frac{T_p}{2\,PI}+\frac{\tau_g}{PI}\leq\eta\leq 1-\frac{\tau_w}{2\,PI}-\frac{T_P}{2\,PI}-\frac{\tau_g}{PI} \quad (3)$$

where τg is a constant guard interval. Note that for the sake of compactness, the dependence of η and P I on t has been ignored.

B. CVPI Sequence Requirement

A spaceborne SAR typically uses a uniform PI sequence based on the timing diagram, with the essential premise that the echoes of interest in the time domain should not overlap with either the transmitted pulses or the nadir echoes. The first and second phenomena to avoid are referred to as transmission blockage and nadir ambiguity, respectively, for the sake of brevity

As a result, when compared to a typical uniform PI sequence, a CVPI sequence is superior because it allows for a significantly larger slant range variation, making it more ideal for an EHR spaceborne sliding spotlight SAR with a large slant range fluctuation, as shown in Fig. 5.

International Journal For Recent Developments in Science & Technology
2581-4575
Crossref
A Peer Reviewed Research Journal

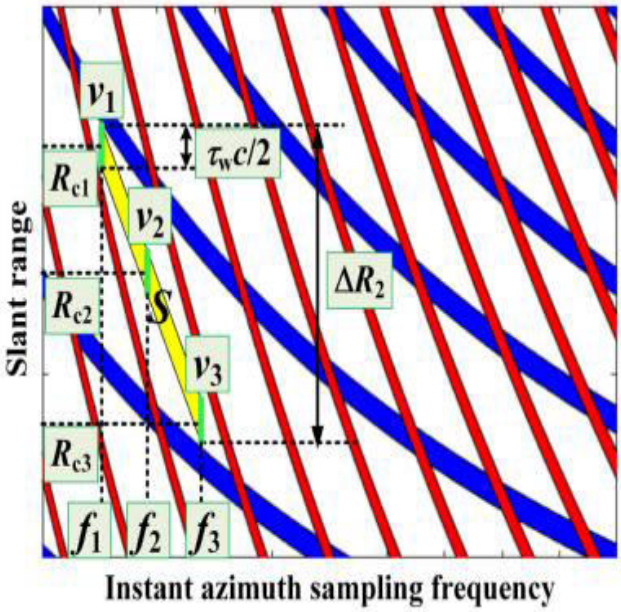

Fig. 7. Presentation of a CVPI sequence in the timing diagram with horizontal axis renamed as the instant azimuth sampling frequency.

we shall refer to the horizontal axis of the timing diagram by the new designation of instant azimuth sampling frequency rather than the original PRF.

However, we now confront a new problem: how do we choose the best CVPI sequence from multiples that satisfy the basic condition

However, we now face a new challenge: how do we choose the optimal CVPI sequence from multiples that meet the fundamental requirement? As a reasonable criterion for optimization, the total required storage memory should be minimized. The total necessary storage memory should be minimised as a fair criterion for optimization. Take, for example, Fig. 7. Of fact, by needing a greater azimuth resolution or a larger azimuth scene extension, it is conceivable to have an even larger slant range variation than R2. For complete data collecting, we can consider using multiple segments of continuous patches, such as S in Fig. 7. This, however, is outside the scope of this essay and will be addressed in a future post.

III. Diagram of strip layering

The goal of this work is to present a new tool for optimum CVPI sequence design called the strip layering diagram. We can intuitively achieve a CVPI sequence by sketching a line segment, rather than an extended patch, in the strip layering diagram with precise control of the movement of the echoes of interest in a pulse train, similar to how we can present a uniform PI sequence by a vertical line segment in the timing diagram. The strip layering diagram's discussion begins with its two components, the candidate sub diagram and the feasibility sub diagram, as shown below.

A. Sub diagram of a Candidate

The main rationale for using a CVPI sequence is to keep the variation of c within bounds such that the transmission blockage and nadir ambiguity requirements are not violated. As an example, consider the uth sample in a CVPI sequence. equation (2) can be rewritten as

$$\tau_c(u) = \mathrm{P\ I}(u)\ \eta\ (u)$$

$$= \frac{2R_c(u-M_e)+\rho(u-M_e)}{c} - \sum_{n=(u-M_e)}^{u-1} PI\ (n)$$

$$\approx \frac{2\,R_c(u)}{c} - M_e \mathrm{P\ I}\ (u) \qquad (4)$$

where Me is the PI number of travelling pulses between transmitting and receiving with respect to the echoes of interest, and is the slant range difference between the two-way journey times. Me should remain unaltered during the data gathering period, as mentioned at the end.

Theoretically, we can suppress the variation of c and, hence, the movement of the echoes of interest in a pulse train by altering the length of PI according to the variation of Rc in (4).A more complete numerical example can be found in Section V-A.

International Journal For Recent Developments in Science & Technology
2581-4575
Crossref
A Peer Reviewed Research Journal

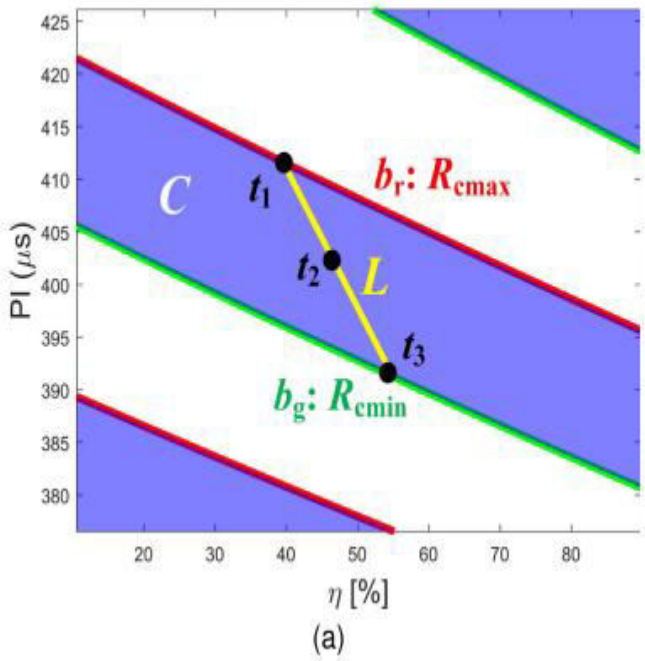

(a)

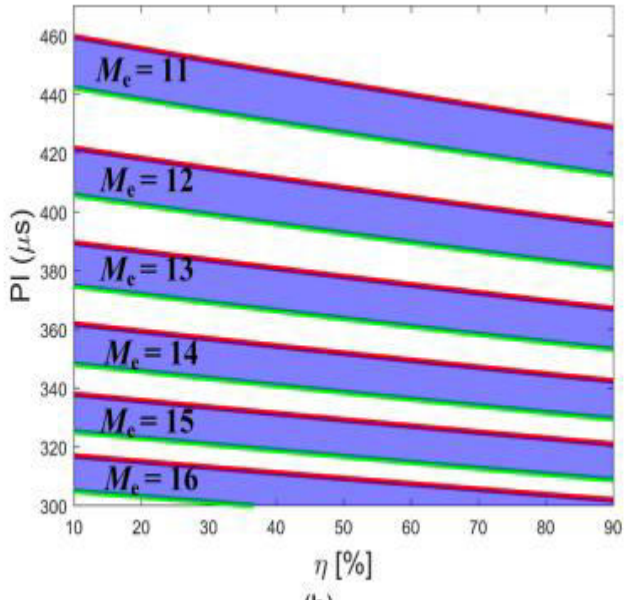

(b)

Fig 8: (a) local and (b) full views of a candidate sub diagram. The diagram in (a) is a zoomed-in version of the diagram in (b)

Consider a new diagram in which the vertical axis is PI and the horizontal axis is, as illustrated in Fig. 8. (a). According to (4), a pair of (P I) maps to a single Rc if a specific Me is specified. As a result, any pairings of (P I,) in a CVPI sequence, such as those at time t1, t2, and t3 in Fig. 8, can be marked in the new diagram (a). A CVPI sequence can be represented by a line segment, such as L in Fig. 8, that connects all of the pairs (P I) during the entire data collecting (a).A single Rc, on the other hand, can be mapped from several pairs of (P I,) as shown in (4).

B: Feasibility

In the temporal domain, a valid CVPI sequence must also meet the basic condition that no part of the echoes of interest overlaps with either the transmitted pulses or the nadir echoes. The feasibility subdiagram is obtained by highlighting all pairings of (P I,) satisfying the fundamental condition in the same coordinate as in Fig. 8(a), indicating that all feasible regions a line segment can be securely sketched within.

The relative delays of the front and rear ends of an echo of interest to the beginning of the PI (the centroid of the most previous transmitted pulse), denoted by F and E, respectively, in Fig. 9, are calculated using the definitions in (2) and Fig. 6.

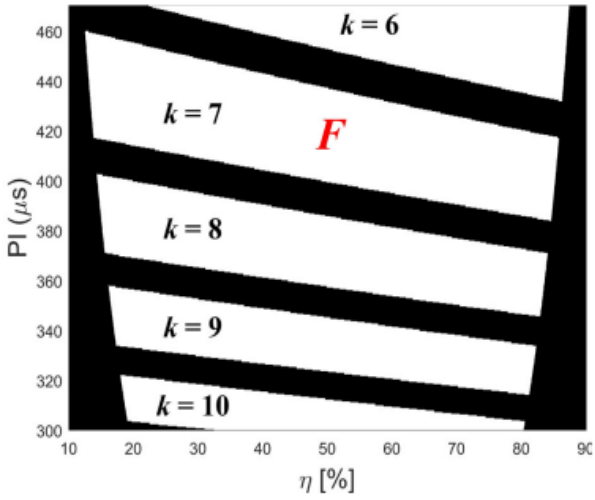

Fig 9: Feasibility sub diagram

where H is the height of satellite orbit, τh is the width of nadir echo, and k is a positive integer.

C. CVPI Sequence Design Using Strip Layering Diagrams

1) Selection criteria:

The final strip layering diagram in Fig. 11 is obtained by layering the candidate subdiagram in Fig. 8 onto the feasibility subdiagram in Fig. 10. Especially to clearly highlight the overlapping relationship with the feasibility strips, the

International Journal For Recent Developments in Science & Technology
2581-4575
Crossref
A Peer Reviewed Research Journal

candidate strips are tinted semitransparent. For the sake of clarity, the red and green hues of the candidate strip boundaries in Fig. 8 have been eliminated as well. The places where a valid CVPI sequence can be securely sketched are indicated by the overlapped parts between the candidate strips and the feasability strips.

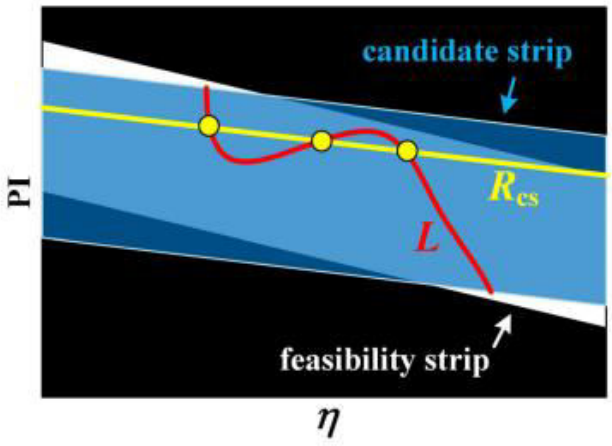

Fig 10: Illustration for a line segment intersectingthe iso-Rcs line at multiple points in the strip layering diagram

1) being fully located at an overlapping region formed by a candidate strip and a feasibility strip;
2) connecting the upper and lower boundaries of a candidate strip at the two nodes;
3) having only one intersection point with an arbitrary isoRc line;
4) causing the echoes of interest in a pulse train to move as little as possible.
The smallest displacement of the echoes of interest in a pulse train is achieved by retaining the product of P I and as a constant G as shown in Fig. 6

$$P\,I\,\eta = G \qquad (5)$$

$$\Pi = \frac{cM_eG}{2\,R_{c-cG}} \qquad (6)$$

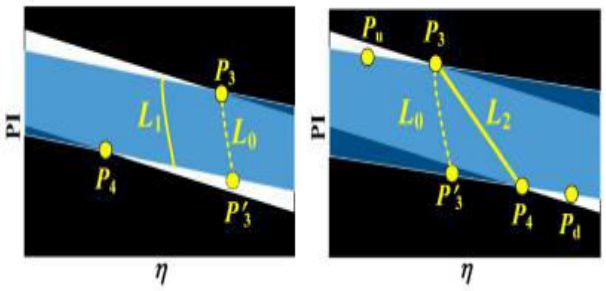

Fig11:CVPI sequences that are optimal in terms of (a) hyperbola line segment L1 and (b) oblique straight-line segment L2.

$$\eta_2 = \frac{cM_ePI_{1\eta 1}}{2R_{cmin} - cPI_{1\eta 1}} \qquad (7)$$

$$PI_{d\eta d} - PI_u\eta_u$$

$$= M_e(PI_u - PI_d) - \frac{2(R_{cmax} - R_{cmin})}{c}$$

$$= M_e(PI_3 - PI_4) - \frac{2(R_{cmax} - R_{cmin})}{c} \qquad (8)$$

2) Creating a CVPI Sequence:

We can always describe Rc as a polynomial due to the azimuth continuous beam steering. According to (4), a CVPI sequence should be modelled as a polynomial with the same trend. We may model the dependence of PI on azimuth time as follows if we assume an order of three.

$$PI(t) = \sigma_0 + \sigma_1 t + \sigma_2 t^2 + \sigma_3 t^3 \qquad (9)$$

We may get a PI at every azimuth time instant by solving the coefficients of $\sigma_0\sigma_1\sigma_2\sigma_3$ in (9). As a result, generating the final CVPI sequence is simple.

$$t_i + 1 = t_i + PI(t_i) \qquad (10)$$

Where the i indicates the azimuth sample index

3)Slope of strips:

The manner a legitimate overlapping zone is generated is determined by the relative slopes of the candidate strip and the feasibility strip. The slope of an iso-Rc line can be calculated using (4).

$$\frac{dPI}{\eta I} = -\frac{2\,R_c}{c(\eta + M_e)^2} \qquad (11)$$

International Journal For Recent Developments in Science & Technology
2581-4575
Crossref
A Peer Reviewed Research Journal

$$\frac{dPI}{\eta I}=\frac{R_{cmax}+R_{cmin}}{c(\eta+M_e)^2} \quad (12)$$

$$\frac{dPI}{\eta I} = -\frac{\Omega_1}{c(\eta+k)^2} \quad (13)$$

$$\Omega_1 = \frac{2H}{c} - \frac{T_p}{2} - \frac{\tau_w}{2} \quad (14)$$

$$\frac{dPI}{\eta I} = -\frac{\Omega_2}{c(\eta+k+1)^2} \quad (15)$$

$$\Omega_2 = \frac{2H}{c} - \frac{T_p}{2} + \frac{\tau_w}{2} + \tau_h \quad (16)$$

$$\frac{dPI}{\eta I} = \frac{\Omega_1}{2c(\eta+k)^2} - \frac{\Omega_2}{2c(\eta+k+1)^2} \quad (17)$$

The upper and lower boundaries are denoted by PI_{min} and PI_{max}

$$PI < PI_{max} = \frac{\lambda}{4v_{s\theta}} \quad (18)$$

$$PI > PI_{min} = \tau_w + T_p + 2\tau_g \quad (19)$$

We may get the lowest and maximum integers for Me, represented by Memin and Memax, respectively, by putting P Imax and P Imin into (4).

$$[\frac{2R_{cmin}}{cPI_{max}}] - 1 = \text{Memin} \le M_e \le \text{Memax} = [\frac{2R_{cmin}}{cPI_{min}}] \quad (20)$$

$$[\frac{\Omega_2}{PI_{max}}] - 2 = k_{min} \le k \le k_{max} = [\frac{\Omega_1}{PI_{min}}] \quad (21)$$

IV. Timing diagram comparision

The two graphic tools should theoretically be equivalent because both the strip layering diagram and the timing diagram are based on the same theoretical foundation that a valid PI sequence should avoid any part of the echoes of interest being overlapped with either the transmitted pulses or the nadir echoes. The strip layering diagram, on the other hand, outperforms by attaining an optimum CVPI sequence rather than just a possible one, thanks to its capacity to precisely and effectively regulate the movement of the echoes of interest in a pulse train. In this section, we'll explain how a line segment in a strip layering diagram maps to a standard timing diagram, then analyse why the timing diagram isn't the best tool for conducting research.

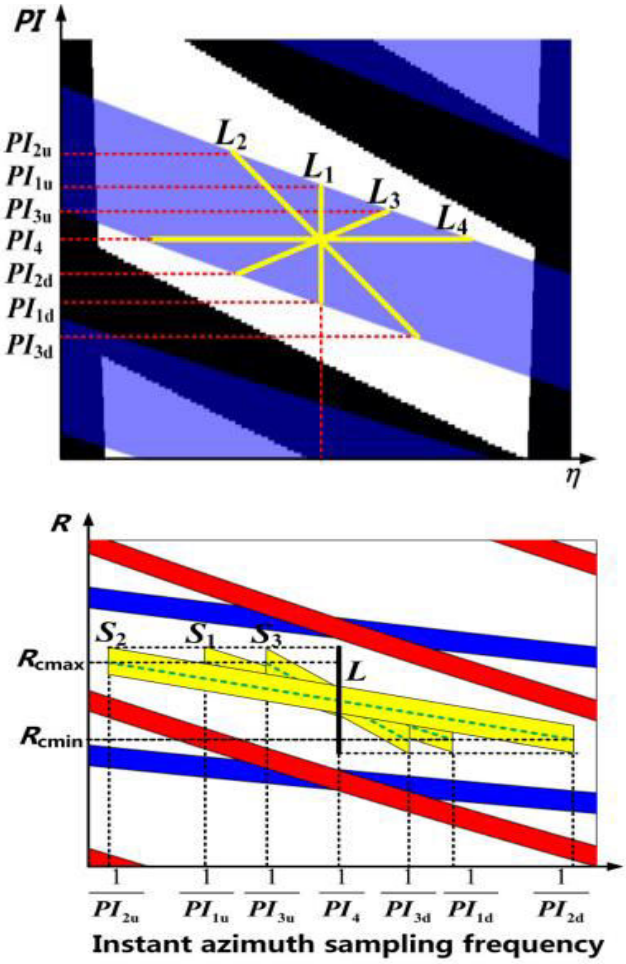

Fig12:(a) strip layering diagram and (b) timing diagram, different forms of PI sequences are presented.

V. Experimental Results:

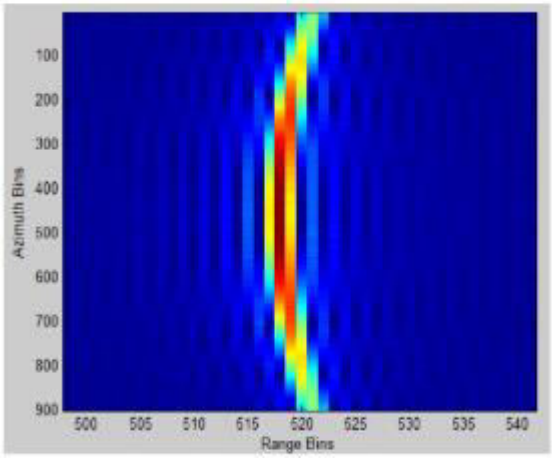

International Journal For Recent Developments in Science & Technology
2581-4575
Crossref
A Peer Reviewed Research Journal

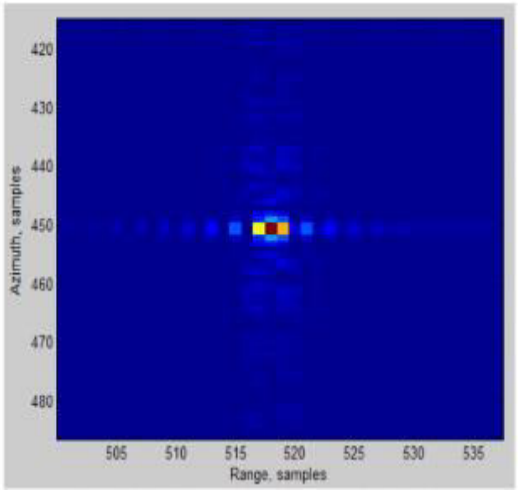

VI. Conclusion:

The SAR imaging simulation is an important step towards the goal of making a process with which realistic SAR images. The modifications to the geometry, echo

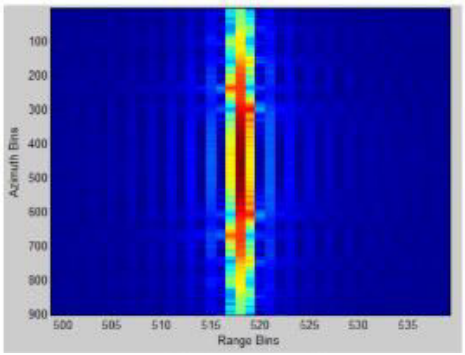

generation were effective in adapting the simulation to an extra dimension. The main effect on simulation result is the modification to range resolution as a function of the look angle and is inversely related to the altitude resolution. Limitations of SAR imaging simulation include target size due to the processing time constraints and line-of-sight point target reflection decisions which restricts the ease which new target profiles can be simulated. The processing time limitation is a carryover from the SAR imaging simulation, which was caused by the processing requirements of the SAR echo generation sequence.

References:

[1] S.-W. Chen, X.-S. Wang, and M. Sato, "Urban damage level mapping based on scattering mechanism investigation using fully polarimetric SAR data for the 3.11 East Japan earthquake," IEEE Trans. Geosci. Remote Sens., vol. 54, no. 12, pp. 6919–6929, Dec. 2016.

[2] Y. Yamaguchi, "Disaster monitoring by fully polarimetric SAR data acquired with ALOS-PALSAR," Proc. IEEE, vol. 100, no. 10, pp. 2851–2860, Oct. 2012.

[3] S.-W. Chen and M. Sato, "Tsunami damage investigation of built-up areas using multitemporal spaceborne full polarimetric SAR images," IEEE Trans. Geosci. Remote Sens., vol. 51, no. 4, pp. 1985–1997, Apr. 2013.

[4] D. Cerutti-Maori, I. Sikaneta, and C. H. Gierull, "Optimum SAR/GMTI processing and its application to the radar satellite RADARSAT-2 for traffic monitoring," IEEE Trans. Geosci. Remote Sens., vol. 50, no. 10, pp. 3868–3881, Oct. 2012.

[5] S. Suchandt, H. Runge, H. Breit, U. Steinbrecher, A. Kotenkov, and U. Balss, "Automatic extraction of traffic flows using TerraSAR-X alongtrack interferometry," IEEE Trans. Geosci. Remote Sens., vol. 48, no. 2, pp. 807–819, Feb. 2010.

[6] D. Cerutti-Maori, J. Klare, A. R. Brenner, and J. H. G. Ender, "Wide-area traffic monitoring with the SAR/GMTI system PAMIR," IEEE Trans. Geosci. Remote Sens., vol. 46, no. 10, pp. 3019–3030, Oct. 2008.

[7] X. X. Zhu, S. Montazeri, C. Gisinger, R. F. Hanssen, and R. Bamler, "Geodetic SAR tomography," IEEE Trans. Geosci. Remote Sens., vol. 54, no. 1, pp. 18–35, Jan. 2016.

[8] M. Eineder, C. Minet, P. Steigenberger, X. Cong, and T. Fritz, "Imaging geodesy—Toward centimeter-level ranging accuracy with

TerraSAR-X," IEEE Trans. Geosci. Remote Sens., vol. 49, no. 2, pp. 661–671, 2011.

[9] X. Cong, U. Balss, M. Eineder, and T. Fritz, "Imaging geodesy— Centimeter-level ranging accuracy with TerraSAR-X: An update," IEEE Geosci. Remote Sens. Lett., vol. 9, no. 5, pp. 948–952, 2012.

[10] G. Farquharson, W. Woods, C. Stringham, N. Sankarambadi, and L. Riggi, "The capella synthetic aperture radar constellation," in Proc. IEEE Int. Geosci. Remote Sens. Symp., Jul. 2018, pp. 1873–1876.

v